Fracture Mechanics of Concrete and Concrete Structures - High Performance, Fiber Reinforced Concrete, Special Loadings and Structural Applications- B. H. Oh, et al. (eds)
© 2010 Korea Concrete Institute, ISBN 978-89-5708-182-2

Fracture properties of high-strength steel fiber concrete

W.-J. Kim, M.-S. Kwak & J.-C. Lee
Kyungpook National University,Korea

ABSTRACT: This study presents the fracture properties of steel fiber concrete. The ratio and notch length of steel fiber in concrete beam specimens, with dimensions of 10cm×10cm×40cm, were selected as independent parameters for the identification of the properties. The volume ratio of steel fiber in the concrete specimen was changed from 0% to 0.5%, 0.75% and 1%. The notch length was changed from 0 mm to 15, 30 and 45 mm. By applying three-point bending tests, J-integral (J_{Ic}), K_{Ic}, G_F, deflection strength, and fracture energy were obtained. Sensitivity analysis was performed to identify the behavior of the dependent variables by changing the volume ratio of steel fiber in the concrete specimen.

1 INTRODUCTION

Ordinary concrete has many microcracks, which degrade and damage the concrete structure along with the cracks that appear during service. Such cracks consequently cause many problems to the entire structure. In particular, stress-related concrete fracturing is directly responsible for structural collapse, and studies are required to address this problem.

Therefore, the safety performance of the structure cannot be reasonably evaluated only by concrete strength, but requires the evaluation of the final limit state behavior, which is the softening behavior. Randomly distributed microcracks initially form upon the application of load to the concrete structure or material. Such microcracks show nonlinear behavior with stable crack growth area before the load reaches its maximum and have the fracture characteristic that the fracture process zone is big relative to the fracture length. Even after the application of maximum load, the fracture has softening behavior with sufficient load transfer capability. This can be explained via the fracture mechanics based on the energy concept, instead of on the existing strength theory.

In this study, the fracture energy, which is the parameter for the representation of the fracture characteristic in the virtual fracture model, was mainly used. The virtual fracture model was proposed by Hillerborg et al. The RILEM equation was used as the concrete fracture mechanics experiment method.

2 RESEARCH SIGNIFICANCE

When tensile stress is applied to SFRC, its tensile strength and ductility significantly increased compared with those of normal concrete. For concrete with steel fiber content of 1.5%, the tensile strength of SFRC is about 30–40 % higher than that of normal concrete. The SFRC has high tensile strength and ductility because of the pullout-resistant mechanism of steel fiber wherein the steel fiber in the concrete controls the crack propagation due to the tensile stress and resists the tensile stress across the crack. In addition, increasing the steel fiber content and the subsequent increase in the number of steel fibers per unit area control the crack propagation. Accordingly, the tensile strength, strain under maximum tensile stress, ductility and fracture energy increase.

2.1 *Virtual Crack Model*

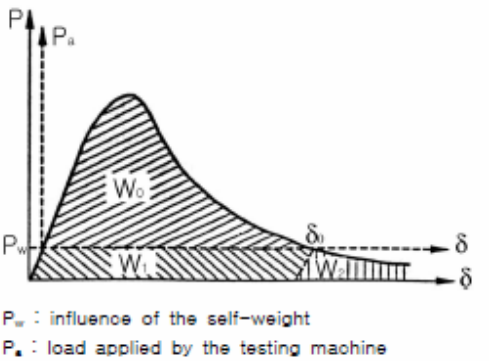

Figure 1. Determination of fracture energy GF.

This study mainly used fracture energy, which is the parameter for the representation of the fracture characteristic in the virtual fracture model.

The virtual fracture model was proposed by Hillerborg et al. The method recommended by RILEM was used as the concrete fracture mechanics

experiment method. The virtual crack model involves three parameters: fracture energy (G_F), material tensile strength (f_t), and critical crack displacement (w_c). In the recommended method, however, the determination of fracture energy is mostly addressed. The characteristic length (lch), which is determined by combining G_F and f_t, is known to be a pure material characteristic and is reportedly proportional to the length of the fracture process zone. In the virtual crack model, the fracture energy can be calculated by dividing the area below the load–displacement curve in Figure 1 by the specimen's cross-section, according to Equation 1.

$$G_F = \frac{W_0 + 2P_w\delta_0}{(b-a_0)t} \quad (1)$$

3 EXPERIMENT AND MATERIAL CHARACTERISTIC EVALUATION METHOD

In this study, the concrete specimen was manufactured with ordinary Portland cement and fiber-reinforced concrete (0.5%, 0.75% and 1%). From the load–CMOD curve obtained from the three-point bending test, Young's modulus (E), critical effective crack length (a_c), critical stress intensity factor (K^s_{IC}), critical crack tip opening displacement ($CTOD_c$), fracture energy (G_F) and characteristic length (Q) were calculated and their correlations were examined.

3.1 *Materials*

Domestic class-1 ordinary Portland cement was used in this experiment. Tables 3.1 and 3.2 show the cement's physical and chemical material properties.

Table 3. 1 Chemical composition of the cement.

Component	Sio_2	Al_2O_3	Fe_2O_3	MgO	SO_3	CaO	K_2O	Na_2O
Composition Ratio (%)	21.4	7.0	2.9	3.1	1.7	60.8	0.72	0.12

Table 3. 2 Physical properties of the cement.

Specific Gravity	Fitness (cm2/g)	Setting Time		Compressive Strength (Kgf/cm2)		
		Ini	Fin	3d	7d	28d
3.15	3.140	225	440	210	280	376

Table 3. 3 Physical properties of the aggregate.

Classt	Specific Gravity	Gmax (mm)	Unit Weight (Kg/m_2)	Absorption(%)	F.M
F.A	2.58	5	1564	1.05	2.91
C.A	2.66	15	1569	0.9	6.49

River sand from Haepyeongsan, Gyeongbuk, and crushed aggregate from Pyeongeunsan were used as aggregate in this experiment. The physical properties were reviewed according to the test method KS F 2502 – 2506. Table 3.3 shows the results.

The steel fiber concrete of domestic manufacturer S was used in this study. The steel fiber was used at volume ratios of 0.5%, 0.75% and 1% of the binder. Table 3.4 shows the physical properties.

Table 3. 4 Physical properties of steel fiber.

Type		Diameter (mm)	Length (mm)	Aspect ratio	Specific gravity (g/m^3)	Tensile strength (MPa)
Double Hook		0.7	50	71.43	7.85	1,100

Table 3. 5 Concrete content table.

Type	W/B	Fiber (%)	Unit Weight (kg/m^3)				
			Water	Binder	Sand	Aggregate (Kg)	Air Entering
NF	20%	0	626	1124	325	675	2.4g
SFC1		0.5					
SFC2		0.75					
SFC3		1					

Binder = Cement + Silica + Fly ash
S/A(%) = 33%, Notch = 0,15,30,45mm

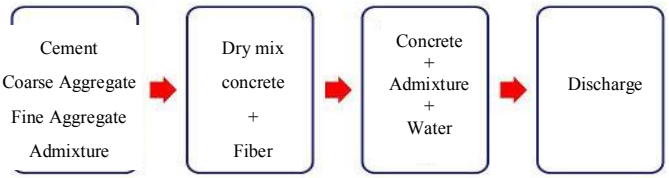

Figure 2. Concrete mixture.

Concrete was mixed in manufacturing the test specimen using a forced mixer, according to the sequence shown in Figure 2. After the dry mixing, fiber was manually and uniformly scattered and dry mixing was performed again. To identify the unhardened concrete characteristic, the slump and flow were measured. In addition, the Φ50×100 mm specimen was manufactured and cured in water at 23±2℃, and its compressive strength was measured on the 28th day.

The test specimen for the three-point bending test on a notched beam was a 100mm×100mm×400mm rectangular parallelepiped with notches 15 mm, 30 mm and 45 mm deep and 5 mm wide, which were made using an electric saw.

Table 3.5 shows the concrete's composition

The compressive strength, tensile strength and elastic modulus were measured as the basic mechanical characteristics of the cylindrical concrete test specimen. Each test was performed according to KS F 2405, KS F 2423 and KS F 2438.

3.2 *Experiment Method*

Figure 3. Three-point bending test on a notched beam.

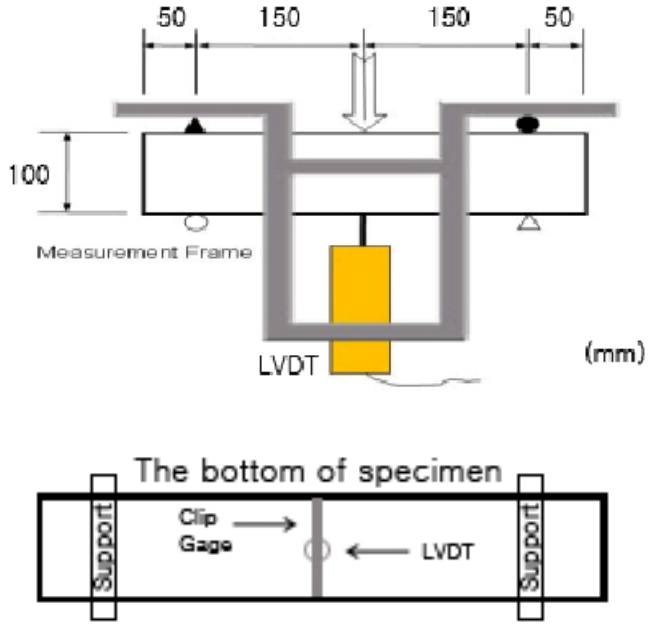

Figure 4. Shape of the notched beam test specimen and displacement measurement position.

In the three-point bending test, the motor connected to the screw jack was rotated at a constant speed to maintain the displacement of the force application head attached to the screw jack at 1 mm/min. A balance with an allowable load of 10 tons was used to measure the load.

Vertical displacement was measured using a 1.0×10^{-6}m-sensitivity displacement meter that was attached to the center of the specimen span, and the CMOD was measured using a 5.5×10^{-6}m-sensitivity clip gauge attached to the thickness-wise end of the beam span center notch. As local fracturing of the test specimen could affect actual displacement during vertical displacement measurement, a frame for measuring the displacement was manufactured. (Fig. 3)

3.3 *Material Property Evaluation Method*

From the three-point bending test on a notched beam, the load–deflection curve and load–CMOD curve were obtained.

Figure 5 shows the representative graphs for each test specimen. From the load–displacement curve, effective bending strength, elastic modulus and fracture energy were calculated according to the following equations.

(1) Effective bending strength

$$\sigma_{net} = \frac{3L_p S}{2W(D-a_0)^2} \tag{2}$$

D:depth, W:width W:width, σ0=initial notch length, S:span, Lp=peak Load

(2) Elastic modulus

$$E = \frac{6Sa_0 v_1(\alpha)}{c_I d^2 b} \tag{3}$$

C_I = Initial loading compliance

$$V_1(\alpha) = 0.76 - 2.28\alpha + 3.87\alpha^2 - 2.04\alpha^3 + \frac{0.66}{(1-\alpha)^2} \qquad \alpha = a_0 / D$$

(3) Fracture energy (G_F)

The fracture energy is calculated by dividing the area below the load–displacement curve until the load reaches zero by fractured area. The area below the curve is calculated by integration.

$$G_F = \frac{U}{A} \tag{4}$$

(4) Specific fracture energy (G_{Fs})

$$G_{Fs} = \frac{W_s}{A_{lig}} \tag{5}$$

W_s=Fs-CMOD Curve integration
A_{lig}=Crack area

4 TEST RESULTS AND ANALYSIS

Graphs in Figures 5–12 show the relationship between the CMOD and deflection according to the load and notch lengths (0, 5, 15, 30 and 45 mm). CMOD and deflection were measured by the unit of 1.0 mm.

4.1 *Test Results of the Cylindrical Test Specimen Material Characteristic*

The following are the test results of the compressive strength, tensile strength and elastic modulus of the cylindrical test specimen.

4.2 *Three-Point Bending Test Results*

Table 4.1 shows the results of the three-point bending test on a notched beam.

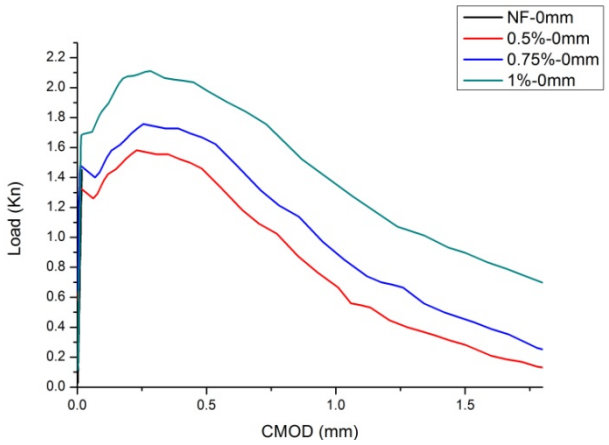

Figure 5. CMOD–Load Curve (notch = 0mm).

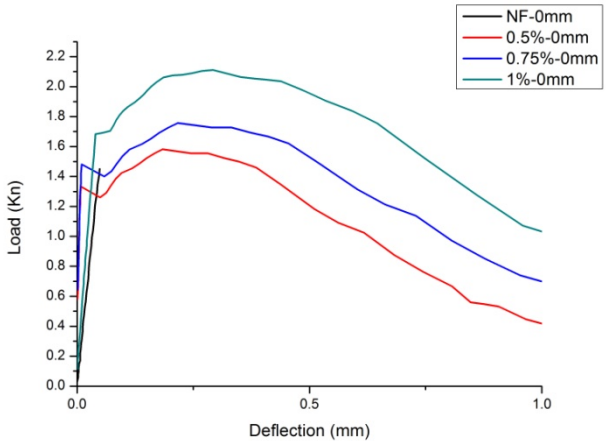

Figure 6. Deflection–Load Curve (notch = 0mm).

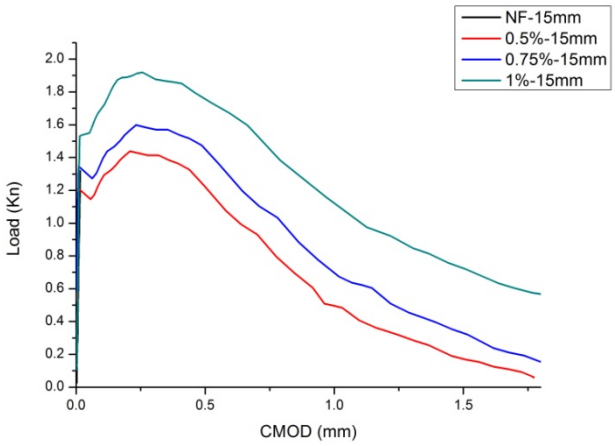

Figure 7. CMOD–Load Curve (notch = 15mm).

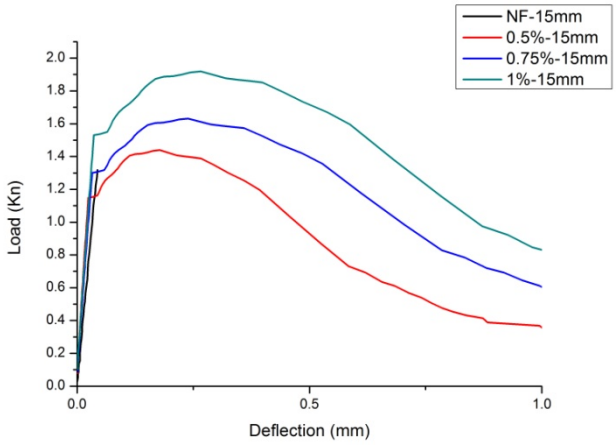

Figure 8. Deflection–Load Curve (notch = 15mm).

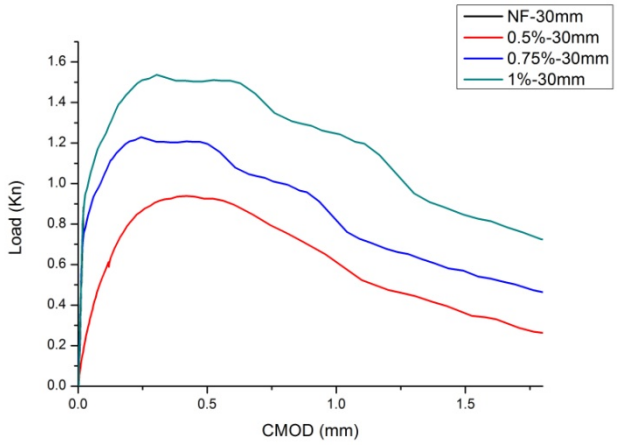

Figure 9. CMOD–Load Curve (notch = 30mm).

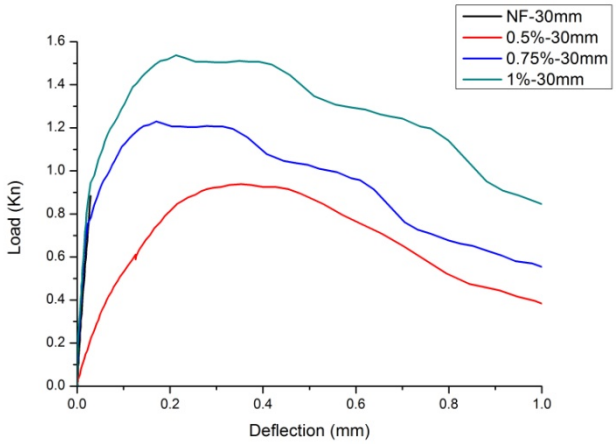

Figure 10. Deflection–Load Curve (notch = 30mm).

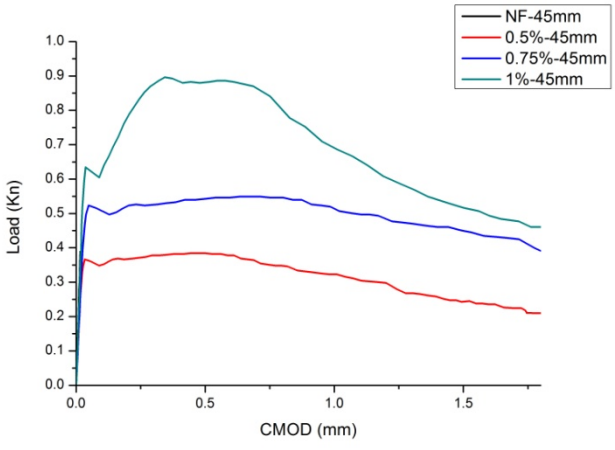

Figure 11. CMOD–Load Curve (notch = 45mm).

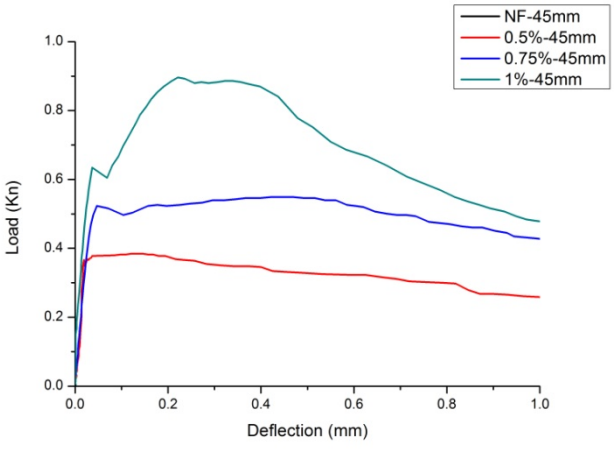

Figure 12. Deflection–Load Curve (notch = 45mm).

Table 4. 1 Characteristic values of the cylindrical test specimen.

Type Notch	Type	D (mm)	a_0 (mm)	α_0 (a_0/d)	d- a_0 (mm)
0mm	NF	100	0	0	100
	SFC1	101	0	0	101
	SFC2	100	0	0	100
	SFC3	102	0	0	102
15mm	NF	100	15	0.150	85
	SFC1	101	15	0.148	86
	SFC2	99	15	0.151	84
	SFC3	101	15	0.148	86
30mm	NF	101	30	0.297	71
	SFC1	100	30	0.3	70
	SFC2	101	30	0.297	71
	SFC3	100	30	0.3	70
45mm	NF	102	45	0.441	57
	SFC1	101	45	0.445	56
	SFC2	100	45	0.450	55
	SFC3	101	45	0.445	56

Table 4. 2 Characteristic values of the cylindrical test specimen.

Type	Number	C.S. (MPa)	T.S. (MPa)	E. (GPa)
NF (Plain)	1	58.8	5.80	28.5
	2	50.5	5.20	24.3
	3	56.7	5.49	26.7
SFC1 0.5%	1	53.7	5.35	24.8
	2	58.3	5.46	26.2
	3	52.5	5.24	24.5
SFC2 0.75%	1	54.4	5.42	26.1
	2	67	6.81	33.2
	3	54.2	5.52	26.0
SFC3 1%	1	67.5	6.56	33.4
	2	63.2	6.42	31.2
	3	67.3	6.85	33.3

C.S : Compressive Strength, T.S : Tensile Strength

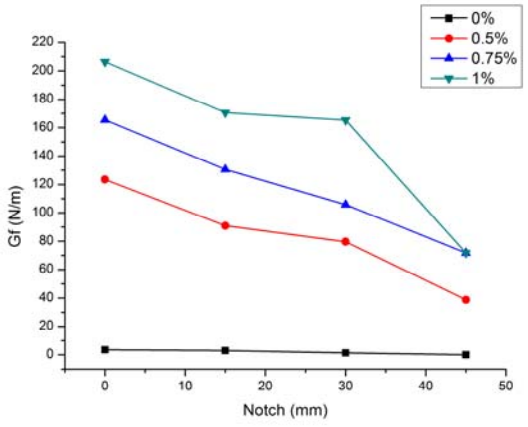

Figure 14. Fracture energy by mixed fiber content.

4.3 *Results and Review*

The average values from the test were used for the result graphs, and the following results were obtained.

The greater amount of fiber content (0%, 0.5%, 0.75% or 1%) resulted in higher fracture energy, as shown in Figure 13. As shown in the figure, the longer notch length resulted in less fracture energy.

The deviation between the fracture energy obtained from the three-point bending test on a notched beam and the nominal fracture energy was somewhat high, but they were roughly proportional to each other.

5 CONCLUSION AND FUTURE STUDIES

To evaluate the fracture energy characteristic of the concrete according to the mixed fiber content, the three-point bending test on a notched beam was performed with varying fiber contents (0%, 0.5%, 0.75% and 1%) and different notch lengths (0, 15, 30 and 45) as variables. The test results showed that the fiber content increases the concrete fracture energy.

The following are the results of this study and further studies required in the future.

(1) It was determined that fiber mixed with concrete increased the concrete fracture energy. It seems that the SFRC has high tensile strength and ductility due to the pullout-resistant mechanism of steel fiber wherein the steel fiber in the concrete controls the crack propagation due to the tensile stress and resists the tensile stress across the crack.

(2) The concrete fracture energy increased for the higher fiber content and shorter notch length. This seems to have been due to the increase in steel fiber content and the subsequent increase in the number of steel fibers per unit area that controlled the crack propagation, and therefore, the tensile

strength, strain under maximum tensile stress, ductility and fracture energy increased. In addition, it seems that the longer notch length was, the lower the fracture energy due to the acceleration of crack propagation.

(3) In the future, further studies involving fiber type and aspect ratio will be required.

6 ACKNOWLEDGMENTS

The work presented in this paper was supported by the Ministry of Education & Human Resources Development through the Second Stage of BK21.

REFERENCES

Alford, N. M., Groves, G. W., and Double, D. D *"Physi cal Properties of High-Strength Cement Pastes", Cement and Concrete Research*, V.12, No.2, May 1982, pp.349–358.

B. trunk. G. Schober, A.K. Gelbing. F.H. Wittmann *"Fracture mechanics parameters of autoclaved aerated concrete"* Cement and Concrete Research 29. 1999, pp. 58–66.

Bazant, Z. P. & Celdolin. L. *"Blunt Crack band Propagation in Finite Element Analysis"*, Journal of Eng. Mechanics. DIV. ASEC vol. 105. No. EN2, 1979 pp. 337–342.

Choi, Sin-Ho *"The Fracture of Concrete according to the Maximum Size of Coarse Aggregate by 3PBT and WTT"*, Architectural Institute of Korea. No. 174, 2003 pp. 97–104.

energy and strain softening of AAC. RILEM *Technical Recommendations for the testing and use of construction materials E & FN Spon*,1994, pp 156–158.

Griffth, A. A., *"The Phenomena of Rupture and Flow in Soilds"* Philosophical Transaction, Royal Society of London Vol. A22, 1921, pp. 163–198.

Hillerbor. A., M.Modeer & P.E. Petersson *"Analysis of Crack Formulation and Crack Growth in Concrete by means of Fracture Mechnics Finite Elements"*, Cement and Concrete Research Vol. 6, 1976, pp.773–782.

K.K. Sideris, P. Manita, E. Chaniotakis, *"Performance of thermally damaged fiber-reinforced concretes,"* Construction and Building Materials 23 (2009), pp. 1232–1239.

Muhammad N.S. Hadi, *"Behaviour of eccentric loading of FRP confined fibre steel reinforced concrete columns"*, Construction and Building Materials 23 (2009), pp.1102–1108.

Qingduo Hao, Yanlei Wangb, Zheng He, Jinping Ou *"Bond strength of glass fiber reinforced polymer ribbed rebars in normal strength concrete",* Construction and Building Materials, 23 (2009), pp. 865–871.

RILEM Recommendation AAC13.1. Determination of the specific fracture